ACS APPLIED MATERIALS & INTERFACES

Research Article

www.acsami.org

Design of a Novel Cu_2O/TiO_2/Carbon Aerogel Electrode and Its Efficient Electrosorption-Assisted Visible Light Photocatalytic Degradation of 2,4,6-Trichlorophenol

Yabo Wang, Ya-nan Zhang, Guohua Zhao,* Hongyi Tian, Huijie Shi, and Tianchen Zhou

Department of Chemistry, Tongji University, Siping Road 1239, Shanghai 200092, PR China

ABSTRACT: Cu_2O/TiO_2 heterojunction photocatalyst is built on carbon aerogel (CA) substrate with good adsorption properties by sol impregnation and seed-mediated synthesis approach. The Cu_2O/TiO_2/CA electrode has excellent electrosorptive and high efficient photocatalytic properties. Its morphology and surface chemical composition are characterized with SEM, TEM, X-ray diffraction (XRD) and Raman spectra. The UV−vis diffuse reflectance spectra show that the optical absorption edge for Cu_2O/TiO_2/CA appears at 636 nm. Under visible-light (λ > 420 nm) irradiation, the photocurrent density increment on Cu_2O/TiO_2/CA is 60 times of that on Cu_2O/TiO_2/FTO. The electrochemical characteristic is investigated with electrochemical impedance spectrum (EIS). The Cu_2O/TiO_2/CA electrode is further applied in the electrosorptive photodegradation of the 2,4,6-trichlorophenol (2,4,6-TCP) wastewater. The result shows that the removal ratio of 2,4,6-TCP in 5.5 h on Cu_2O/TiO_2/CA is 96.3% and the TOC removal is 91.3%. The intermediates generated in the degradation process are analyzed by GC-MS and HPLC. The possible mechanism of visible light photocatalytic degradation of 2,4,6-TCP on Cu_2O/TiO_2/CA is also studied.

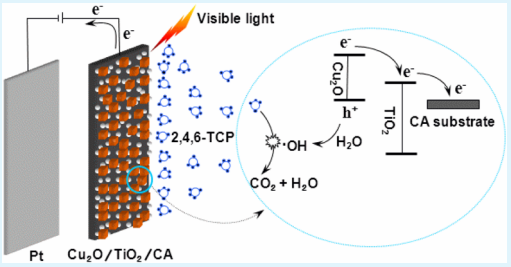

KEYWORDS: *Cu_2O/TiO_2/carbon aerogel electrode, p−n heterojunction, electrosorption-assisted visible light photocatalysis, 2,4,6-trichlorophenol, degradation mechanism, intermediate products*

1. INTRODUCTION

In recent years, the semiconductor photocatalytic oxidation technology has been widely used in wastewater treatment because of its simple operation, mild reaction conditions, and no secondary pollution.[1−5] Among many semiconductor photocatalysts, TiO_2 is one of the most effective photocatalysts with a wide band gap energy, excellent chemical, photo corrosion resistance, low price, and nontoxicity properties.[6−10] The notable advances have been made over the past two decades. However, the quantum efficiency of TiO_2 is low. And only UV light can be absorbed by TiO_2, which leads to low utilization of solar energy. Studies have shown that n-type TiO_2 combined with p-type semiconductor to form a heterojunction photocatalyst is an effective way to improve the photocatalytic efficiency.[11−13] In recent years, Cu_2O combined with TiO_2 has become a research hotspot.[14,15] Cu_2O is a p-type semiconductor with a narrow band gap of 2.1 eV. Because of the matching of the band structure between Cu_2O and TiO_2, photogenerated electrons are transferred from the conduction band (CB) of Cu_2O to the CB of TiO_2. Besides, the built-in electric field originated from the Cu_2O/TiO_2 heterojunction also favors the separation of photogenerated electron−hole.

However, a few problems still exist. First, the electro-hole pairs remain easy to recombine and the quantum efficiency is still low. If the photogenerated charges cannot be transferred in time, the accumulated electrons and holes will be recombined leading to the reduction of the photocatalytic activity. Second, the accumulated holes might cause the photocorrosion of Cu_2O since it is a narrow band semiconductor.

Carbon aerogel (CA) is an outstanding electrosorption material with high specific surface area and well conductivity and arouses extensive attention from scientists in recent years.[16] The high surface area of CA is in favor of the growth of nanomaterials. Moreover, the good conductivity of CA leads to a fast electronic transmission between the semiconductor and CA. So CA can become an ideal electrode substrate material.

Herein, we propose to build Cu_2O/TiO_2 p−n heterojunction photocatalysts on the surface of the CA by seed-mediated and sol impregnation synthesis approach. The Cu_2O/TiO_2/CA electrode material is expected to receive excellent electric adsorption properties and efficient photocatalytic properties. The advantages of this electrode are as follows. First, the three-dimensional network structure of CA substrate can endow the TiO_2 and Cu_2O photocatalysts with high loading capacity and surface area. The more p-n heterojunction formed between TiO_2 and Cu_2O can lower the recombination of photoinduced charges. Therefore the quantum efficiency of the photocatalyst will be greatly improved. Second, the electro-hole pairs are effectively separated because of the well conductivity of CA and the applied low bias. Third, Cu_2O/TiO_2/CA is a block electrode material. When it is applied to the electrosorption-

Received: May 7, 2012
Accepted: July 10, 2012
Published: July 10, 2012

 © 2012 American Chemical Society dx.doi.org/10.1021/am300795w | ACS Appl. Mater. Interfaces 2012, 4, 3965−3972

assisted degradation of pollutants under visible light, the high concentration of pollutants is absorbed on the catalyst surface due to the excellent electrosorption properties of CA. And the reaction rate of the photocatalytic process is greatly enhanced. The efficient degradation of pollutants is achieved by the synergistic effect between electrosorption, p−n heterojunction and photocatalysis.

In this paper, Cu_2O/TiO_2/CA electrode is applied to treat a simulated 2,4,6-trichlorophenol (2,4,6-TCP) wastewater in an electrosorption-assisted visible light photogradation process. 2,4,6-TCP has been widely used as pulp bleaching, disinfectant, pesticide and wood preservative. It has been reported to cause adverse effects on human nervous system and respiratory problems. And the uncontrolled use and disposal of 2,4,6-TCP has led to serious impact on surface water quality. As one type of the most hazardous materials, 2,4,6-TCP is carcinogenic, mutagenic and resistant to biodegradation.[17−21] The treatment performance and the mechanisms involved with degradation of 2,4,6-TCP are investigated and compared with traditional Cu_2O/TiO_2/FTO electrode. This work provides an effective theoretical basis to deal with environment pollutants by using solar energy, and has important theoretical and applied value.

2. EXPERIMENTAL SECTION

2.1. Preparation of Cu_2O/TiO_2/CA Electrode. CA was prepared by sol−gel process at ambient pressure drying, which had been reported in our previous study.[22] TiO_2 nanoparticles were loaded on CA by sol−gel approach. Titanium tetrabutylate, ethanol and acetylacetone (volume ratio of 1:3:0.1) were mixed and stirred at ambient conditions under magnetic stirring. Then, a mixture containing nitrate acid, deionized water and ethanol (volume ratio of 1:4:20) was added. After it was stirred for 2 h, the CA was immersed in the sol for 30 min. Then, the CA was placed inside an oven at 90 °C for 1 h. The above steps were repeated three times. The substrate was calcined at 500 °C for 3 h in nitrogen atmosphere. The electrode was calcined at a heating rate of 1 °C min^{-1} to the desired temperature, then cooled to room temperature. Cu_2O nanoparticles were loaded on TiO_2/CA using a seed-mediated synthesis approach. In a typical procedure, a volume of 10 mL aqueous solution containing 1×10^{-3} M copper sulfate ($CuSO_4 \cdot 5H_2O$) and 3.3×10^{-2} M sodium dodecyl sulfate (SDS) was prepared and transferred to a bottle labeled A with one piece of TiO_2/CA electrode. The other bottle labeled B was added to 9 mL of the same solution. Then 250 μL of 0.2 M sodium ascorbate was added into bottle A and shaken for 5 s, followed by the addition of 500 μL of 1 M NaOH. After shaking the solution for another 5 s, 1 mL of this solution and the TiO_2/CA electrode were transferred to bottle B. Then 250 μL of sodium ascorbate was added and shaken for 5 s and 500 μL of 1 M NaOH was added and shaken for another 5 s. On standing at room temperature for 2 h, the electrode was placed inside an oven at 50 °C for 1 h. The amount of the catalysts was measured by difference method (difference of the electrode quality before and after the loading).

2.2. Characterization of the Surface Structure and Physicochemical Properties. The morphology of catalyst is characterized by the field emission environmental scanning electron microscopy (FE-SEM, Hitachi S4800) and the transmission electron microscopy (TEM, JEM-2100, JEOL) with an accelerating voltage of 200 KV. The Cu_2O sample for TEM characterization is prepared by the following step. Very small amount of Cu_2O nanoparticles are scraped from Cu_2O/TiO_2/CA and put into ethanol for ultrasonic dispersion. The crystal structure of catalyst is characterized by the X-ray diffraction analysis (XRD, Bruker Co., Ltd., Germany). Raman spectra of the electrodes were recorded with a Raman spectrometer (InVia, Renishaw). The specific surface areawas calculated by Brunauer−Emmett−Teller (BET) method (TRISTAR 3000 Micromeritics). The electrical properties of hybrids are tested on a micromanipulator manual probe station in the dark. The Cu_2O and TiO_2 film are loaded on FTO, respectively. The $I-V$ characterization is to determine the formed p-n junction between Cu_2O and TiO_2 film.

Photoelectrochemical properties are measured in the three-electrode system of CHI660C electrochemical workstation. Cu_2O/TiO_2/CA and Cu_2O/TiO_2/FTO work as anode, platinum plate as the counter electrode, and saturated calomel electrode as the reference electrode. Electrochemical impedance spectroscopy (EIS) is used to determine the conductivity of the electrodes, with the frequency range from 1×10^5 to 1×10^{-3} Hz and amplitude 5 mV. The electrolyte is 0.005 M $[Fe(CN)_6^{3-}]/[Fe(CN)_6^{4-}]$ solution. Photocurrent density is measured in 0.05 M Na_2SO_4. A 500 W xenon lamp (center wavelength 420 nm, light intensity 150 mW cm^{-2}) is used as the visible light source.

2.3. Degradation Experiment. Degradation experiment was carried out in a round reaction pool, in which water was recycled in order to maintain the reaction temperature at 25 °C. The Cu_2O/TiO_2/CA and Cu_2O/TiO_2/FTO worked as the anode, platinum plate as the counter electrode, and saturated calomel electrode as the reference electrode. Electrode area was 5.5 cm^2, electrode spacing was 1.0 cm. A 500 W xenon lamp (center wavelength 420 nm, light intensity 150 mW cm^{-2}) is used as the visible light source. The anode potential was held at 0.5 V. 100 mL solution containing 150 mg L^{-1} 2,4,6-TCP was used as the simulated wastewater.

The concentration of 2,4,6-TCP was tested by HPLC (Varian 3900 HPLC). The samples are detected and quantified by AQ-C18 (4.6 × 100 mm, 5 μm) and UV detector at λ = 210 nm. 5:95 (v/v) acetonitrile/phosphate buffer (pH 2.3) is employed as the mobile phase at the flow rate of 0.8 mL min^{-1}, and the injection volume was 20 μL. The aromatic intermediates were analyzed by the Eclipse XDB-C18 and selected UV detector at λ = 270 nm. 30:70 (v/v) methanol/water was employed as the mobile phase at the flow rate of 0.5 mL min^{-1}. Generated carboxylic acids were analyzed by the Eclipse XDB-C18 and selected UV detector at λ = 230 nm. 20:80 (v/v) methanol/water was employed as the mobile phase at the flow rate of 0.5 mL min^{-1}. GC-MS (Agilent 6890GC, Agilent 5973MSD) was used to determine the intermediates qualitatively. The gaseous phase separation of intermediates was performed in the capillary column (Agilent HP-5MS, 30 m × 0.25 mm × 0.25 μm), and injection volume of 1 μL. The temperature of capillary column starts from 328.15 to 513.15 K at a rate of 8 K min^{-1} and hold time 5 min. The organic components of about 100 mL of the 2,4,6-TCP solution treated with Cu_2O/TiO_2/CA anode for 60 min were extracted three times with 100 mL of CH_2Cl_2. The collected organic solution was dried with molecular sieves (3 Å), filtered and concentrated to 2 mL.

3. RESULTS AND DISCUSSION

3.1. Morphology and Surface Characteristics. Figure 1 shows the SEM and TEM images of the electrodes. In Figure 1A, the CA has network structure consisting of granular nanoparticles. The carbon spheres are in the same diameter about dozens of nanometers, and the whole network structure is relatively loose. Figure 1B is the SEM image of TiO_2/CA electrode. TiO_2 nanoparticles are evenly loaded in the pores of CA. The size of TiO_2 nanoparticles is about 15 nm, and there is no obviously intense aggregation. Cu_2O is fully dispersed on the surface of TiO_2/CA (Figure 1C). It can be seen from Figure 1D that Cu_2O has cubic structural with an edge length about 50 nm. The loading weight of TiO_2 and Cu_2O are 0.0878 and 0.0674 g, respectively.

The crystal structure of the electrode is studied by X-ray diffraction analysis (XRD) (Figure 2A). The two diffraction peaks of CA (curve a) is the reflection of C(002) and C(101).[23,24] For TiO_2/CA electrode (curve b), the diffraction peaks with 2θ values of 25.6, 37.8, 48.1, 55.1, and 62.7 correspond to (101), (004), (200), (211), (204) crystal planes of anatase TiO_2 (JCPDS card No. 04−0477), respectively. For Cu_2O/TiO_2/CA electrode (curve c), the diffraction peaks with

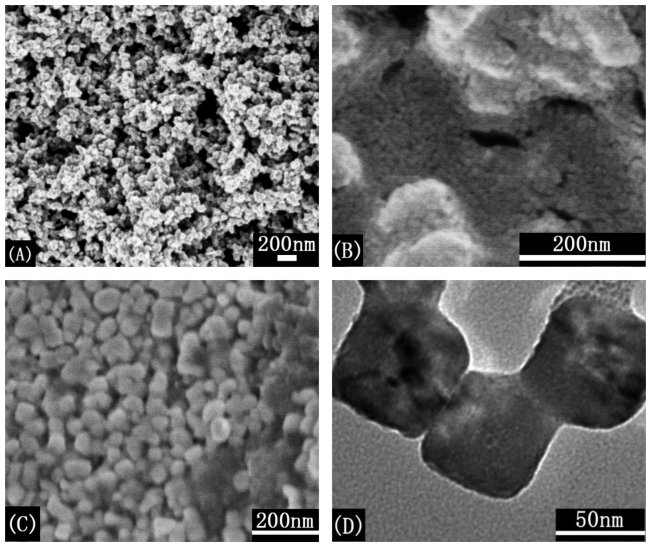

Figure 1. SEM images of (a) CA, (b) TiO_2/CA, (c) Cu_2O/TiO_2/CA, and (d) TEM images of Cu_2O.

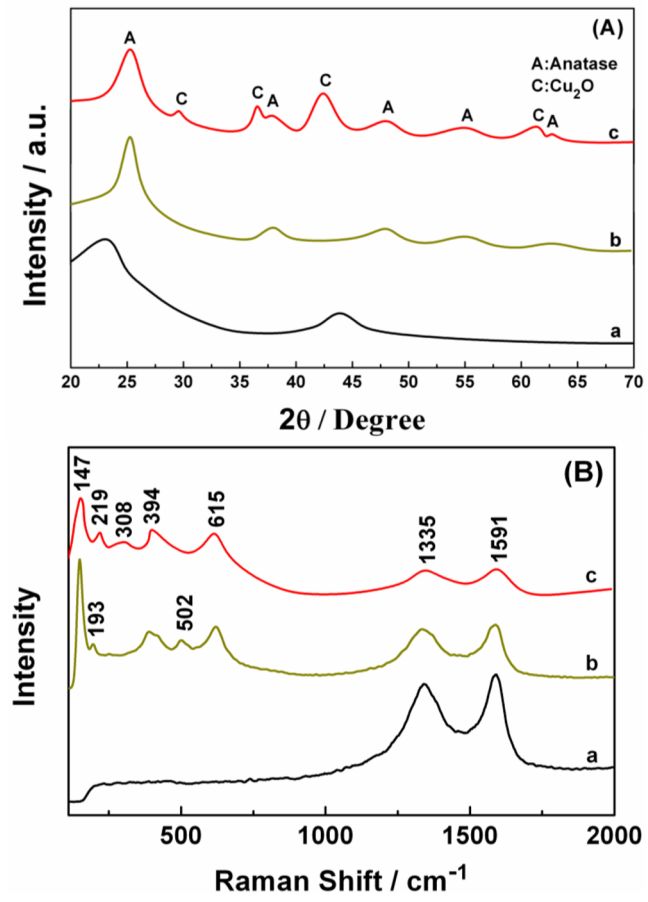

Figure 2. (A) XRD patterns of (a) CA, (b) TiO_2/CA, and (c) Cu_2O/TiO_2/CA; (B) Raman spectra of (a) CA, (b) TiO_2/CA and (c) Cu_2O/TiO_2/CA.

2θ values of 29.6, 36.5, 42.4, and 61.5 correspond to (110), (111), (200), (220) crystal planes of pure cubic Cu_2O (JCPDS card No. 05−0667), respectively. It is confirmed that the anatase TiO_2 and cubic Cu_2O are successfully loaded on the CA substrate. The Raman spectra results displayed in Figure 2B. For TiO_2/CA (curve b), there are five strong vibration peaks at 147 cm^{-1} (E_g), 193 cm^{-1} (E_g), 394 cm^{-1} (B_{1g}), 502 cm^{-1} (A_{1g}), and 615 cm^{-1} (E_{1g}) attributed to the five Raman active modes ($A_{1g} + B_{1g} + 3E_g$) of anatase.[25,26] Two peaks at 1335.3 and 1590.5 cm^{-1} are attributed to the graphite crystallites D and G of CA (curve a).[27,28] For Cu_2O/TiO_2/CA (curve c), the peaks at 147 cm^{-1} (E_g), 394 cm^{-1} (B_{1g}), and 615 cm^{-1} (E_{1g}) are attributed to the Raman active modes of anatase of TiO_2. Two peaks at 219 and 308 cm^{-1} are the two second-order overtones of Cu_2O.[29] The characteristic peaks of graphite crystallites in CA also appear. This conclusion is consistent with the XRD.

3.2. Photocatalytic and Electrical Properties Measurement. Figure 3A is the UV−vis spectra of the electrodes. The

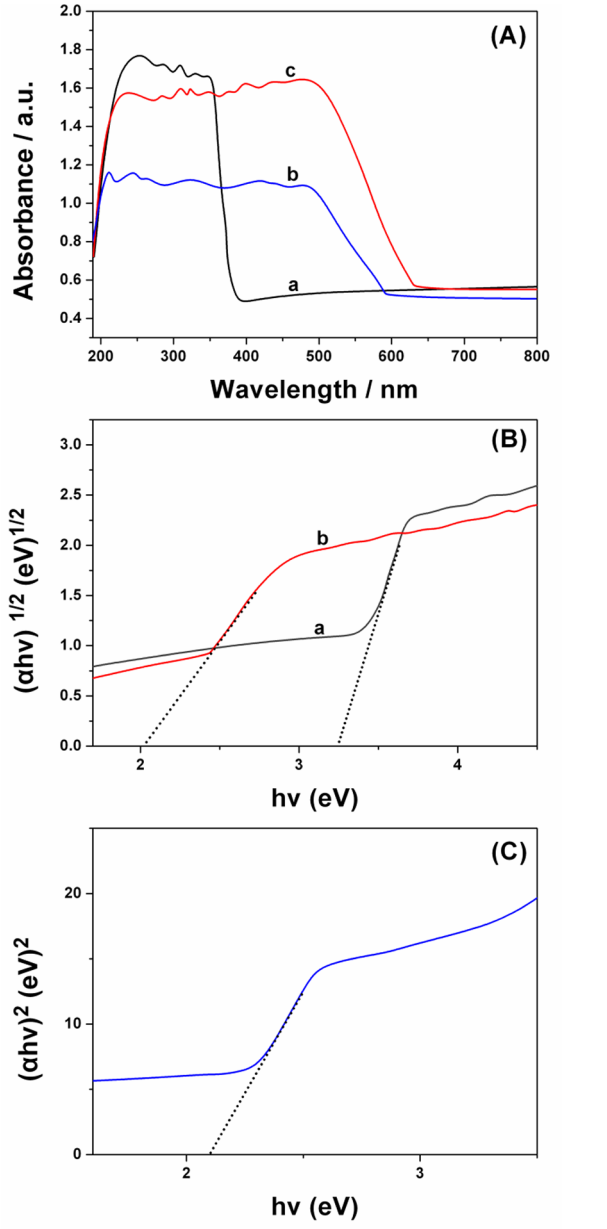

Figure 3. (A) UV−vis diffuse reflectance spectra of (a) TiO_2/CA, (b) Cu_2O/CA, (c) Cu_2O/TiO_2/CA. (B) Plots of the $(\alpha h\nu)^{1/2}$ vs photon energy ($h\nu$) for (a) TiO_2/CA and (b) Cu_2O/TiO_2/CA. (C) Plots of the $(\alpha h\nu)^2$ vs photon energy ($h\nu$) for Cu_2O/CA.

dx.doi.org/10.1021/am300795w | ACS Appl. Mater. Interfaces 2012, 4, 3965−3972

absorption edge of TiO_2/CA (curve a) appears at 386 nm. The UV−vis spectra of TiO_2/CA indicate that the crystal structure of TiO_2 is anatase which is consistent with the XRD and Raman spectra. The absorption edge of Cu_2O/CA (curve b) appears at 590 nm. Compared with TiO_2/CA, the UV−vis spectra of Cu_2O/TiO_2/CA (curve c) reveals a significant shift of the absorption edge toward the visible region, and the absorption edge appears at 636 nm. The band gap energy of a semiconductor could be calculated by the following formula[30,31]

$$\alpha h\nu = A(h\nu - E_g)^{n/2}$$

Where α, ν, E_g, and A are absorption coefficient, light frequency, band gap, and a constant, respectively. Among them, n depends on the characteristics of the transition in a semiconductor. The value of n is 1 for the direct transition of Cu_2O/CA. And the value of n is 4 for the indirect transition of TiO_2/CA and Cu_2O/TiO_2/CA. The band gap energy (E_g value) of the resulting samples can be estimated from a plot of $(\alpha h\nu)^{1/2}$ versus photon energy ($h\nu$) and $(\alpha h\nu)^2$ versus photon energy ($h\nu$). The intercept of the tangent to the X axis would give a good approximation of the band gap energy of the samples. The band gap of Cu_2O/TiO_2/CA (Figure 3B, curve b) is found to be about 1.98 eV, whereas the band gap of TiO_2/CA (Figure 3B curve a) and Cu_2O/CA (Figure 3C) are evaluated to be 3.2 and 2.1 eV, respectively.

Figure 4A identifies the *I*−*V* characteristics of the Cu_2O/TiO_2 film measured with a micromanipulator manual probe station in the dark, whose contact configuration is shown schematically in the inset. The current increases exponentially under a positive bias (Cu_2O positive with respect to TiO_2). While in the negative region (TiO_2 positive with respect to Cu_2O), the reverse current remains very limited. The obvious current asymmetry under the forward and reverse bias directions indicates the formation of p-n heterojunction between TiO_2 and Cu_2O. The heterojunction can promote separation of photoinduced charge carriers, reducing recombination of photogenerated electrons and holes, which will be beneficial to obtain high quantum efficiency. Figure 4B shows the current density on electrodes with 150 mg L^{-1} 2,4,6-trichlorophenol in 0.05 mol L^{-1} Na_2SO_4 solution at 0.5 V potential. When Cu_2O is excited by visible light, the photogenerated electron and hole are produced. The exerted electric field can help the photogenerated electrons move away from the CB of Cu_2O to the CA substrate. The electrons are then quickly guided away under the applied electric field. So the photocurrent is generated. Compared with dark current density, a small current change can be observed for TiO_2/CA. The reasons are as follows. First, it is well-known that anatase TiO_2 do not respond to visible light. In the experiment, we use a filter to screen off UV light and get visible light (λ > 420 nm). A small amount of UV light can still reach to TiO_2/CA electrode because the filtering rate of the filter is 99.5%. Second, CA has excellent electrical conductivity and fast electron transfer. Thus, the sensitive current is easily observed under light irradiation. For Cu_2O/CA (curve b), Cu_2O/TiO_2/FTO (insert) and Cu_2O/TiO_2/CA (curve c), the photocurrent densities all have a significant increase than the dark current density under visible light irradiation. However, the largest increment observed on Cu_2O/TiO_2/CA which is about 2 and 60 times of that on Cu_2O/CA and Cu_2O/TiO_2/FTO. The p−n heterojunction formed between TiO_2 and Cu_2O can decrease

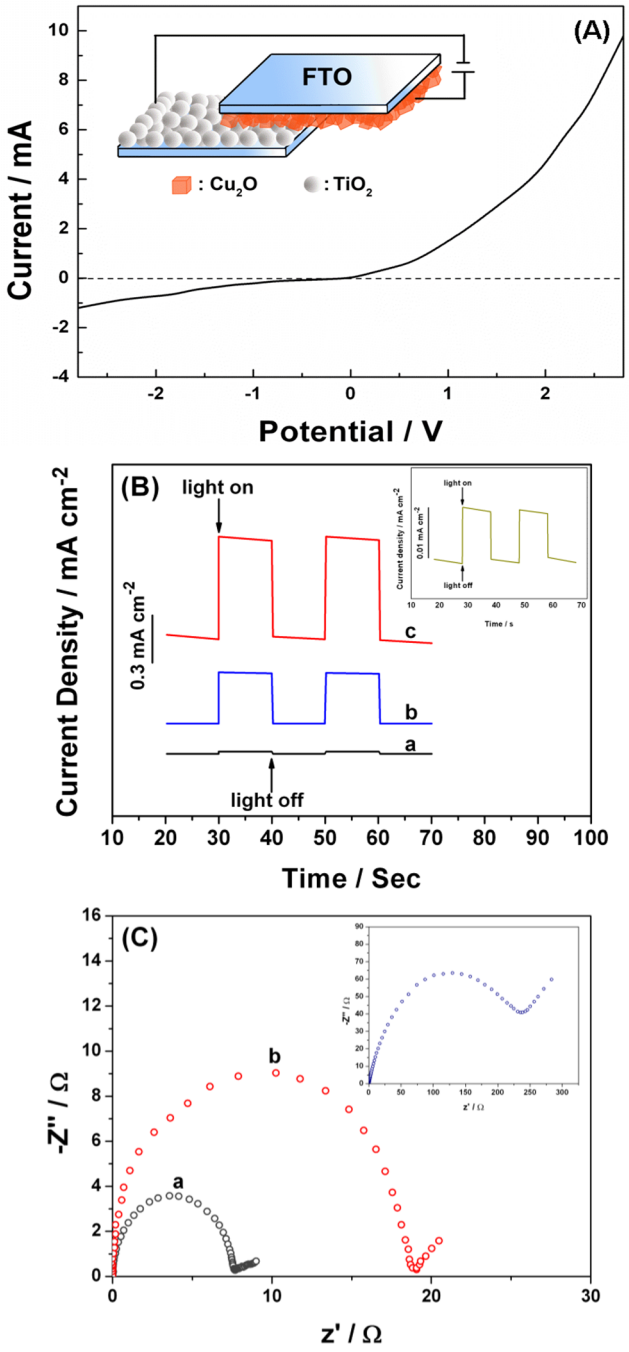

Figure 4. (A) *I*−*V* characteristic of the Cu_2O/TiO_2 film. (B) Comparison of current density for (a) TiO_2/CA, (b) Cu_2O/CA, (c) Cu_2O/TiO_2/CA, and (inset) Cu_2O/TiO_2/FTO. (C) Electrochemical impedance spectroscopy of (a) CA, (b) Cu_2O/TiO_2/CA, and (inset) Cu_2O/TiO_2/FTO.

the recombination of photoinduced charges. Therefore the quantum efficiency of the photocatalyst is greatly improved. In addition, due to the excellent electrochemical properties of CA, the electron transfer is effective and fast which accelerates the electron−hole separation. It indicates that Cu_2O/TiO_2/CA has a stronger photocurrent response. Figure 4C is the electrochemical impedance spectroscopy of electrodes. The electrochemical impedance of CA (curve a) is 7.8 Ω. The electrochemical impedance of Cu_2O/TiO_2/CA (curve b) is 17 Ω after the load of p−n heterojunction. The conductivity of Cu_2O/TiO_2/CA decreases after Cu_2O and TiO_2 nanoparticles

are distributed on the surface of CA (Figure 1C). The electron transfer on the interface of CA and solution is not seriously impeded by the loaded Cu_2O and TiO_2 due to the good conductivity of CA substrate. And the whole $Cu_2O/TiO_2/CA$ electrode still has good conductivity. However, the electrochemical impedance of $Cu_2O/TiO_2/FTO$ (insert) is 236 Ω, the conductivity is greatly affected by the load of p−n heterojunction on FTO.

3.3. Electrosorption-Assisted Visible Light Photocatalytic Degradation of 2,4,6-TCP. Figure 5A is the concentration variation of 2,4,6-TCP with reaction time. Under visible light without the bias, the removal of 2,4,6-TCP on TiO_2/FTO (denoted as TiO_2/FTO, PC. curve a) is very poor. TiO_2 can not respond to visible light, therefore the photoinduced charges can not be produced to oxidative degradation of 2,4,6-TCP. Under the same conditions, the 2,4,6-TCP removal with Cu_2O/FTO (denoted as Cu_2O/FTO, PC. curve b) is 26.8% in 5.5 h. Although Cu_2O can be excited by visible light to produce electrons and holes to oxidative degradation of 2,4,6-TCP, the photoinduced electrons and holes are easy recombination, lowering the activity of the photocatalysts. Furthermore, the accumulated holes have a tendency to induce photocorrosion of the unstable semiconductors.[32,33] Under visible light without bias, the removal of 2,4,6-TCP with Cu_2O/TiO_2/FTO (denoted as Cu_2O/TiO_2/FTO, PC. curve c) and Cu_2O/TiO_2/CA (denoted as Cu_2O/TiO_2/CA, PC. curve d) are 31.6% and 44.9%, respectively. The 2,4,6-TCP removal on Cu_2O/TiO_2/CA is obviously higher than on Cu_2O/TiO_2/FTO. This is due to the Cu_2O/TiO_2/CA electrode has developed three-dimensional network structure and high surface area (627 m^2 g^{-1}). This structure is beneficial for more 2,4,6-TCP adsorption. When the 0.5 V potential and visible light are applied on Cu_2O/TiO_2/FTO (denoted as Cu_2O/TiO_2/FTO, EPC. curve e) and Cu_2O/TiO_2/CA (denoted as Cu_2O/TiO_2/CA, EPC. curve f), in 5.5 h the 2,4,6-TCP removal are 65.8% and 96.3%, respectively. Since Cu_2O/TiO_2/CA electrode has larger surface area and better conductivity than Cu_2O/TiO_2/FTO electrode, the 2,4,6-TCP adsorption capacity of Cu_2O/TiO_2/CA is larger and the transmission rate of electrolyte is quicker, leading to higher treatment efficiency. Figure 5B shows that the TOC removal in Cu_2O/TiO_2/CA, EPC process (91.3% at 5.5 h) is the most efficient technique among four processes. The TOC removal in Cu_2O/TiO_2/CA, EPC process (curve d) is 3.3 times that of Cu_2O/TiO_2/CA, E process (curve a) and 2.5 times that of Cu_2O/TiO_2/CA, PC process (curve b). The TOC removal in Cu_2O/TiO_2/CA, EPC process is higher than the plus of Cu_2O/TiO_2/CA, E process and Cu_2O/TiO_2/CA, PC process. This result shows that the synergistic interaction between the photocatalytic and electrical adsorption. An adsorption-decompose-adsorption circulation forms to prevent the saturated adsorption on the electrode. Therefore, the concentration of 2,4,6-TCP is decreased continuously at high efficiency. The degradation of 2,4,6-TCP had been reported by many scientists.[34−36] In this work, an efficient degradation effect at 5.5 h is obtained on Cu_2O/TiO_2/CA when dealing with high concentrations of 2,4,6-TCP. This work has not been reported. The TOC removal in Cu_2O/TiO_2/CA, EPC process is 1.6 times that of Cu_2O/TiO_2/FTO, EPC process (curve c). The Cu_2O/TiO_2/CA electrode has larger surface area than Cu_2O/TiO_2/FTO, so the 2,4,6-TCP adsorption capacity and the transmission rate of electrolyte are greatly improved. As a result, the efficient oxidation of 2,4,6-TCP is achieved.

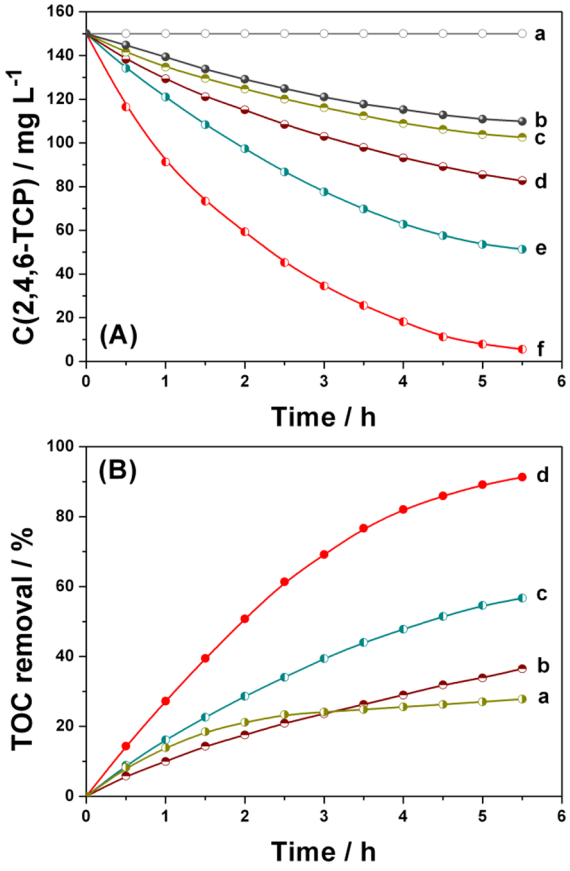

Figure 5. (A) Variation in 2,4,6-TCP concentration with reaction time (at initial 2,4,6-TCP concentration of 150 mg L^{-1} and cathode potential was 0.5 V). (a) TiO_2/FTO, PC, (b) Cu_2O/FTO, PC, (c) Cu_2O/TiO_2/FTO, PC, (d) Cu_2O/TiO_2/CA, PC, (e) Cu_2O/TiO_2/FTO, EPC, (f) Cu_2O/TiO_2/CA, EPC. (B) TOC removal with degradation time: (a) Cu_2O/TiO_2/CA, E, (b) Cu_2O/TiO_2/CA, PC, (c) Cu_2O/TiO_2/FTO, EPC, (d) Cu_2O/TiO_2/CA, EPC.

3.4. Mechanism of Electrosorption-Assisted Visible Light Photocatalytic Degradation. The mechanism (Figure 6) of 2,4,6-TCP degradation is proposed as the following steps. For the semiconductor photocatalytic technology, the generation and separation of the photoinduced electron−hole pairs are the key factors to influence a photocatalytic reaction. At the initial stage, the 2,4,6-TCP molecules are adsorbed onto the electrode surface by electrosorption. Under visible-light

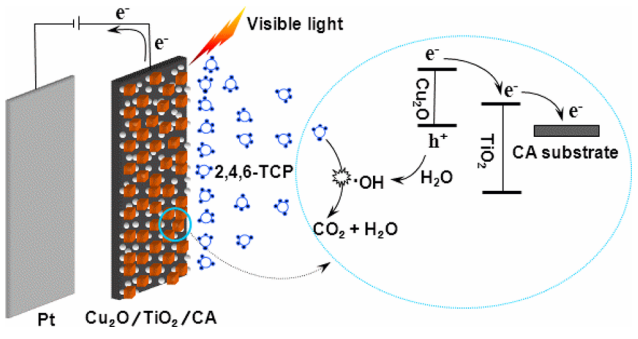

Figure 6. Probable mechanism of the EPC process on Cu_2O/TiO_2/CA electrode.

irradiation, Cu_2O is excited to produce photogenerated electrons and holes. The CB of Cu_2O (−1.4 eV) lies above that of TiO_2 (−0.2 eV), so the photogenerated electrons on the CB of Cu_2O transfer to the CB of TiO_2.[37] And then the electrons are further transferred to the CA substrate. Because CA has good electrical conductivity, electrons are quickly guided away under the applied electric field. Finally, the holes accumulate on the VB of Cu_2O forms hole center. The holes can oxidize the water to form hydroxyl radical (•OH), which has strong oxidation ability to oxidize organic pollutants molecules. On the one hand, the p-n heterojunction formed between TiO_2 and Cu_2O is conducive to the separation of photoinduced charges, reducing the recombination of photogenerated electrons and holes. On the other hand, CA with good electrical conductivity plays the role of rapid conduction electrons under the applied electric field, greatly improving the quantum efficiency of the photocatalyst.

Stable organic intermediate products generated during the degradation process are detected by GC/MS and HPLC, which are identified by comparison with commercial standards. The types of intermediates are some aromatic compounds and small molecule acids. The possible reaction pathway of 2,4,6-TCP degradation can be concluded by the following steps (Figure 7). First, the 2,4,6-TCP molecules are enriched on the surface of $Cu_2O/TiO_2/CA$ electrode by electrochemical adsorption. Then 2,4,6-TCP molecules are oxidized under hydroxyl radical attack to generate a series of aromatic intermediates (such as 2,4-dichlorophenol, 2,6-dichlorophenol, 2,6-dichlorohydroquinone, 2,6-dichloro-1,4-benzoquinone, 2-chlorophenol and 4-chlorophenol). The intermediates are oxidized with the successive attacks of •OH to generate phenol and benzoquinone. Afterward, these aromatic intermediates are further oxidized with the successive attacks by •OH to generate small molecular acid (maleic acid, fumaric acid and oxalic acid). Finally, these intermediates are mineralized to CO_2 and H_2O.

It is known that Cu_2O photocatalyst suffers from photocorrosion in practical application. Thus, it is of great importance to study the stability of $Cu_2O/TiO_2/CA$ during the EPC degradation. The recycled experiments for the degradation of 2,4,6-TCP are performed. As shown in Figure 8, 96.3% of 2,4,6-TCP can be removed within 5.5 h for the first time. After three recycles, 94.2% of 2,4,6-TCP can still be removed by $Cu_2O/TiO_2/CA$ within 5.5 h. These results indicate that the photocorrosion of Cu_2O can be inhibited. When coupling TiO_2 with Cu_2O, the photogenerated electrons on the CB of Cu_2O will transfer to the CB of TiO_2 under visible light irradiation. The accumulating holes on the VB of Cu_2O forms hole center. At this time, the photocorrosion easily occurs because the Cu_2O itself can be oxidized by the hole. When Cu_2O/TiO_2 is loaded on CA, the pollutant concentration on the catalyst surface is very high due to the excellent electric adsorption properties of CA. The absorbed pollutant rather than Cu_2O is preferred to be oxized by the holes on the VB of Cu_2O. Thus the stability of the $Cu_2O/TiO_2/CA$ is accordingly enhanced.

The evolution of some intermediates (phenol, 4-chlorophenol, benzoquinone and maleic acid) concentration is shown in Figure 9. The evolution of four aromatic intermediates is the same in both $Cu_2O/TiO_2/CA$, EPC and $Cu_2O/TiO_2/FTO$, EPC process. The concentrations of aromatic intermediates increase first and then decrease. Accordingly, the time reaching the maximum concentration (C_{max}) is t_{max}. In Cu_2O-TiO_2/CA, EPC process, the C_{max} of phenol, 4-chlorophenol and

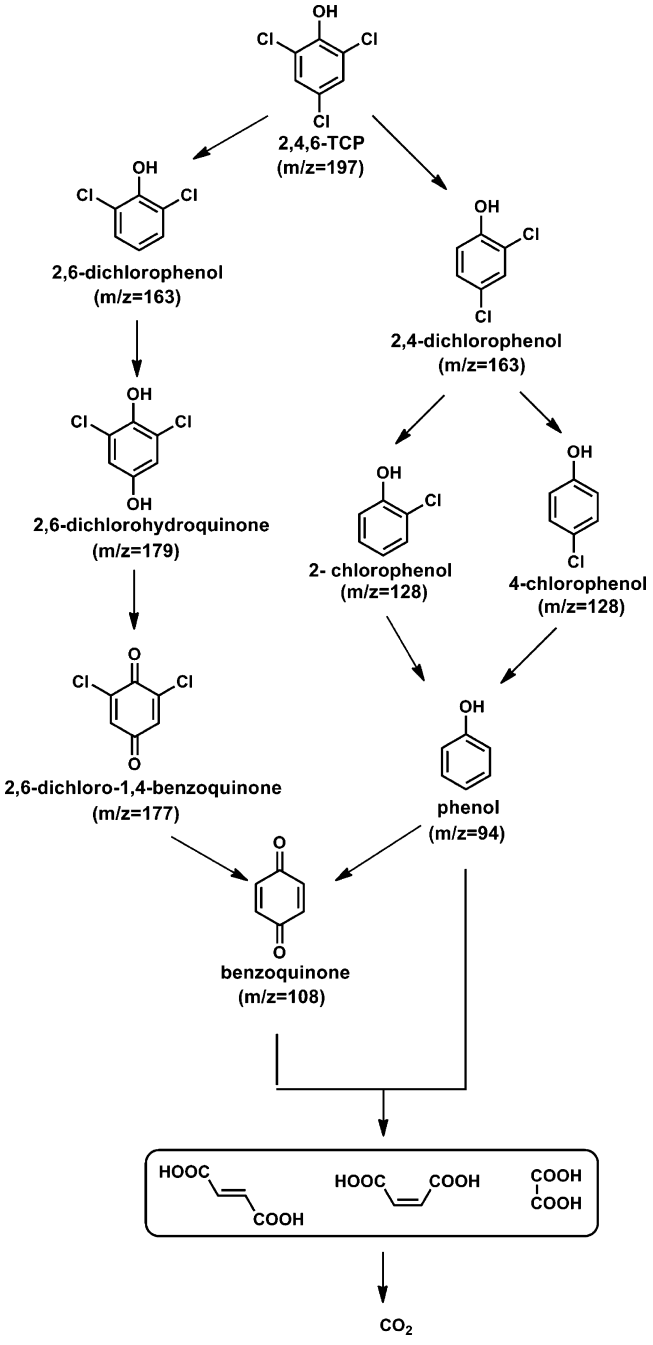

Figure 7. Mechanism of decomposition pathway intermediates of 2,4,6-TCP.

benzoquinone are 9.8, 8.2, and 10.9 mg L^{-1} at 1.5 h, respectively. The C_{max} of maleic acid is 11.6 mg L^{-1} at 2 h. The t_{max} of maleic acid is later than the other three intermediates. Because 2,4,6-TCP is first oxidized under •OH attack to generate aromatic intermediates and then give rise to small molecular acids. In the $Cu_2O/TiO_2/FTO$, EPC process, the t_{max} of phenol, 4-chlorophenol, and benzoquinone is 2 h. The t_{max} of maleic acid is 2.5 h, which is later than in the $Cu_2O/TiO_2/CA$, EPC process. Three-dimensional network structure of CA can significantly increase the load capacity and dispersion of composite nanomaterials. It can make the surface area of photocatalyst significantly increased. Thus more active sites are obtained, enhancing the reaction rate of the photocatalytic process. The four intermediates C_{max} of $Cu_2O/TiO_2/CA$, EPC

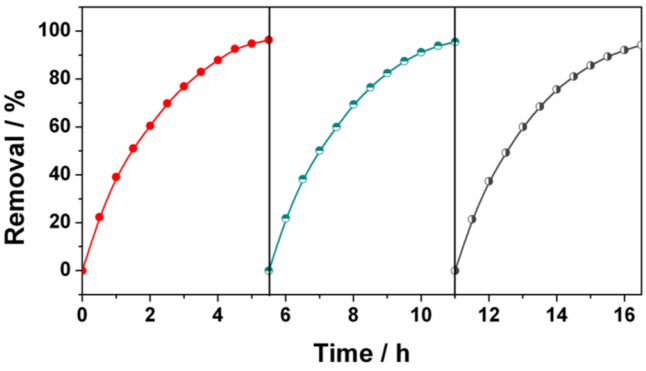

Figure 8. Removal percentage of 2,4,6-TCP after 5.5 h with cyclic EPC degradation.

process are less than Cu_2O/TiO_2/FTO, EPC process. Cu_2O/TiO_2/CA electrode is an excellent electrical absorbent material. Its electrosorption capacity is better than Cu_2O/TiO_2/FTO electrode. By applying a weak electric field, the lower concentration of intermediates can be efficiently adsorbed on the electrode surface and rapidly decomposed. Thus, the number of intermediates diffused into the solution phase is relatively low.

CONCLUSIONS

Cu_2O/TiO_2/CA electrode with excellent electrosorptive and heterojunction photocatalyst was synthesized by loading Cu_2O/TiO_2 p-n heterojunction on CA. The Cu_2O/TiO_2/CA electrode had good conductivity and high specific surface area. The UV−visible spectra showed that the optical absorption edge for Cu_2O/TiO_2/CA appeared at 636 nm. The increment from dark current to the photocurrent density on Cu_2O/TiO_2/CA was about 60 times that on Cu_2O/TiO_2/FTO. The Cu_2O/TiO_2/CA and Cu_2O/TiO_2/FTO electrodes were applied in the degradation of the 2,4,6-TCP wastewater, respectively. The removal ratio of 2,4,6-TCP in 5.5 h was 96.3% and the TOC removal was 91.3% on Cu_2O/TiO_2/CA. The mechanism of 2,4,6-TCP degradation was also fully discussed and analyzed. This study provided a method to exploit highly efficient photocatalysts under visible-light irradiation.

AUTHOR INFORMATION

Corresponding Author

*Tel: (86)-21-65988570-8244. Fax: (86)-21-65982287. E-mail: g.zhao@tongji.edu.cn.

Notes

The authors declare no competing financial interest.

ACKNOWLEDGMENTS

This work was supported jointly by the National Natural Science Foundation of China (21077077, 20877058).

REFERENCES

(1) Li, W. J.; Li, D. Z.; Lin, Y. M.; Wang, P. X.; Chen, W.; Fu, X. Z.; Shao, Y. *J. Phys. Chem. C* **2012**, *116*, 3552−3560.
(2) Qin, H. C.; Li, W. Y.; Xia, Y. J.; He, T. *ACS Appl. Mater. Interfaces* **2011**, *3*, 3152−3156.
(3) Sayama, K.; Hayashi, H.; Arai, T.; Yanagida, M.; Gunji, T.; Sugihara, H. *Appl. Catal., B* **2010**, *94*, 150−157.
(4) Niu, M. T.; Huang, F.; Cui, L. F.; Huang, P.; Yu, Y. L.; Wang, Y. S. *ACS Nano* **2010**, *4*, 681−688.
(5) Xie, Y.; Ali, G.; Yoo, S. H.; Cho, S. O. *ACS Appl. Mater. Interfaces* **2010**, *2*, 2910−2914.
(6) Zhao, W.; Ma, W. H.; Chen, C. C.; Zhao, J. C.; Shuai, Z. G. *J. Am. Chem. Soc.* **2004**, *126*, 4782−4783.
(7) Li, D.; Haneda, H.; Hishita, S.; Ohashi, N. *Chem. Mater.* **2005**, *17*, 2596−2602.
(8) Elahifard, M. R.; Rahimnejad, S.; Haghighi, S.; Gholami, M. R. *J. Am. Chem. Soc.* **2007**, *129*, 9552−9553.
(9) Wang, C. X.; Yin, L. W.; Zhang, L. Y.; Liu, N. N.; Lun, N.; Qi, Y. X. *ACS Appl. Mater. Interfaces* **2010**, *2*, 3373−3377.

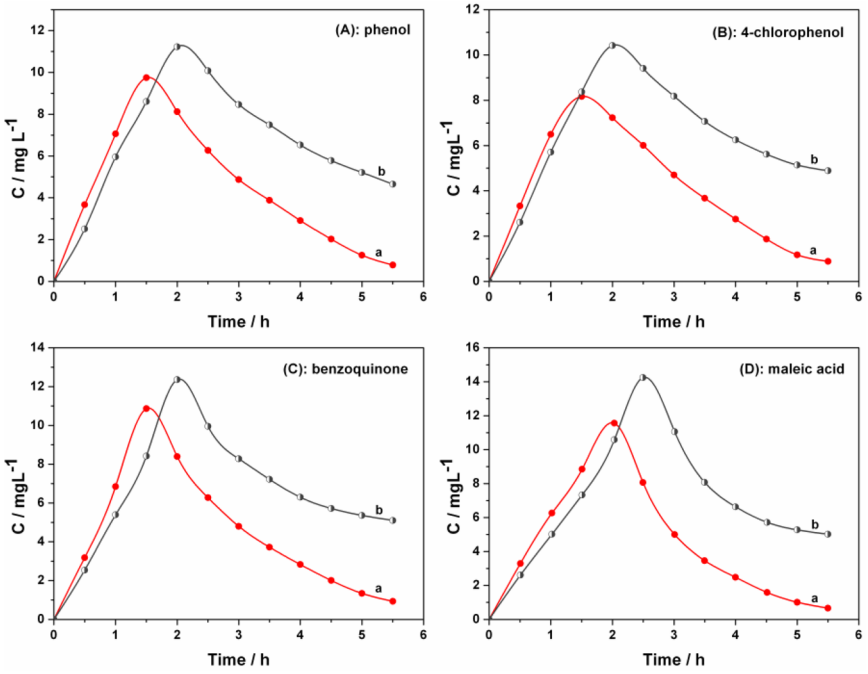

Figure 9. Evolution of intermediate products concentration during degradation of a 150 mg L^{-1} 2,4,6-TCP solution: (a) Cu_2O/TiO_2/CA, EPC; (b) Cu_2O/TiO_2/FTO, EPC.

(10) Lee, W. J.; Lee, J. M.; Kochuveedu, S. T.; Han, T. H.; Jeong, H. Y.; Park, M.; Yun, J. M.; Kwon, J.; No, K.; Kim, D. H.; Kim, S. O. *ACS Nano* **2012**, *6*, 935−943.
(11) Seabold, J. A.; Shankar, K.; Wilke, R. H. T.; Paulose, M.; Varghese, O. K.; Grimes, C. A.; Choi, K.-S. *Chem. Mater.* **2008**, *20*, 5266−5273.
(12) Yu, H. B.; Chen, S.; Quan, X.; Zhao, H. M.; Zhang, Y. B. *Environ. Sci. Technol.* **2008**, *42*, 3791−3796.
(13) Liu, W.; Chen, S. F.; Zhang, S. J.; Zhao, W.; Zhang, H. Y.; Yu, X. L. *J. Nanopart. Res.* **2010**, *12*, 1355−1366.
(14) Yang, L. X.; Luo, S. L.; Li, Y.; Xiao, Y.; Kang, Q.; Cai, Q. Y. *Environ. Sci. Technol.* **2010**, *44*, 7641−7646.
(15) Zhang, J. Y.; Zhu, H. L.; Zheng, S. K.; Pan, F.; Wang, T. M. *ACS Appl. Mater. Interfaces* **2009**, *1*, 2111−2114.
(16) Goel, J.; Kadirvelu, K.; Rajagopal, C.; Garg, V. K. *Ind. Eng. Chem. Res.* **2005**, *44*, 1987−1994.
(17) Christoforidis, K. C.; Serestatidou, E.; Louloudi, M.; Konstantinou, I. K.; Milaeva, E. R.; Deligiannakis, Y. *Appl. Catal., B* **2011**, *101*, 417−424.
(18) Chu, W.; Rao, Y. F.; Kwan, C. Y.; Choy, W. K. *Ind. Eng. Chem. Res.* **2009**, *48*, 10211−10216.
(19) Xiong, Z. G.; Xu, Y. M.; Zhu, L. Z.; Zhao, J. C. *Langmuir* **2005**, *21*, 10602−10607.
(20) Choi, J. H.; Kim, Y. H. *J. Hazard. Mater.* **2009**, *166*, 984−991.
(21) Wang, Y. S.; Shan, X. Q.; Feng, M. H.; Chen, G. C.; Pei, Z. G.; Wen, B.; Liu, T.; Xie, Y. N.; Owens, G. *Environ. Sci. Technol.* **2009**, *43*, 5726−5731.
(22) Wu, M. F.; Jin, Y. N.; Zhao, G. H.; Li, M. F.; Li, D. M. *Environ. Sci. Technol.* **2010**, *44*, 1780−1785.
(23) Nagaoka, S.; Hamasaki, Y.; Ishihara, S.-i.; Nagata, M.; Iio, K.; Nagasawa, C.; Ihara, H. *J. Mol. Catal. A: Chem.* **2002**, *177*, 255−263.
(24) Liu, Y. Z.; Yang, S. G.; Hong, J.; Sun, C. *J. Hazard. Mater.* **2007**, *142*, 208−215.
(25) Wang, H. E.; Zheng, L. X.; Liu, C. P.; Liu, Y. K.; Luan, C. Y.; Cheng, H.; Li, Y. Y.; Martinu, L.; Zapien, J. A.; Bello, I. *J. Phys. Chem. C* **2011**, *115*, 10419−10425.
(26) Ji, Y. J.; Lin, K. C.; Zheng, H. G.; Liu, C. C.; Dudik, L.; Zhu, J. J.; Burda, C. *ACS Appl. Mater. Interfaces* **2010**, *2*, 3075−3082.
(27) Du, X. S.; Yu, Z. Z.; Dasari, A.; Ma, J.; Mo, M. S.; Meng, Y. Z.; Mai, Y. W. *Chem. Mater.* **2008**, *20*, 2066−2068.
(28) Patakfalvi, R.; Diaz, D.; Santiago-Jacinto, P.; Rodriguez-Gattorno, G.; Sato-Berru, R. *J. Phys. Chem. C* **2007**, *111*, 5331−5336.
(29) Wu, L. L.; Tsui, L. K.; Swami, N.; Zangari, G. *J. Phys. Chem. C* **2010**, *114*, 11551−11556.
(30) Cheng, H. F.; Huang, B. B.; Dai, Y.; Qin, X. Y.; Zhang, X. Y. *Langmuir* **2010**, *26*, 6618−6624.
(31) Wu, G. S.; Nishikawa, T.; Ohtani, B.; Chen, A. *Chem. Mater.* **2007**, *19*, 4530−4537.
(32) Bessekhouad, Y.; Robert, D.; Weber, J. V. *Catal. Today* **2005**, *101*, 315−321.
(33) Zheng, Z. K.; Huang, B. B.; Wang, Z. Y.; Guo, M.; Qin, X. Y.; Zhang, X. Y.; Wang, P.; Dai, Y. *J. Phys. Chem. C* **2009**, *113*, 14448−14453.
(34) Díaz-Díaz, G.; Celis-García, M.; Blanco-López, M. C.; Lobo-Castañón, M. J.; Miranda-Ordieres, A. J.; Tuñón-Blanco, P. *Appl. Catal., B* **2010**, *96*, 51−56.
(35) Vijayan, P.; Mahendiran, C.; Suresh, C.; Shanthi, K. *Catal. Today* **2009**, *141*, 220−224.
(36) Anandan, S.; Vinu, A.; Mori, T.; Gokulakrishnan, N.; Srinivasu, P.; Murugesan, V.; Ariga, K. *Catal. Commun.* **2007**, *8*, 1377−1382.
(37) Hou, Y.; Li, X. Y.; Zou, X. J.; Quan, X.; Chen, G. H. *Environ. Sci. Technol.* **2009**, *43*, 858−863.